1,2-CF bond activation of perfluoroarenes and alkylidene isomers of titanium. DFT analysis of the C–F bond activation pathway and rotation of the titanium alkylidene moiety

José G. Andino, Hongjun Fan, Alison R. Fout, Brad C. Bailey, Mu-Hyun Baik*, Daniel J. Mindiola*

Department of Chemistry, Indiana University, Bloomington, IN 47405, USA

ABSTRACT

Isomeric alkylidene complexes *syn*- and *anti*-(PNP)Ti=[C^{t}Bu(C$_6$F$_5$)](F) (**1**) and (PNP)Ti=[C^{t}Bu(C$_7$F$_7$)](F) (**2**) have been generated from C–F bond addition of hexafluorobenzene (C$_6$F$_6$) and octafluorotoluene (C$_7$F$_8$) across the alkylidyne ligand of transient (PNP)Ti≡C^{t}Bu (**A**) (PNP$^-$=N[2-P(CHMe$_2$)$_2$-4-methylphenyl]$_2$), which was generated from the precursor (PNP)Ti=CH^{t}Bu(CH$_2^t$Bu). Two mechanistic scenarios for the activation of the C–F bond by **A** are considered: 1,2-CF addition and [2 + 2]-cycloaddition/β-fluoride elimination. Upon formation of the alkylidenes **1** and **2**, the kinetic and thermodynamic alkylidene product is the *syn* isomer, which gradually isomerizes to the corresponding *anti* isomer to ultimately establish an equilibrium mixture (when using **1**, 65/35) if the solution is heated in benzene to 105 °C for 1 h. Single crystal X-Ray crystallographic data obtained for the two isomers of **2** (and *syn* isomer of **1**) are in good agreement with computed DFT-optimized models. Our calculations suggest convincingly that the isomerization process proceeds via a concerted rotation involving a heterolytic bond cleavage about the alkylidene bond. The two rotamers are thermodynamically very close in energy and interconvert with an estimated barrier of ∼26 kcal/mol. The electronic reason for this unexpectedly low barrier is investigated.

1. Introduction

Carbon–fluorine bond activation in aromatic substrates continues to be a challenge in organotransition metal chemistry for multiple reasons. With a typical bond strength of ∼154 kcal/mol the carbon fluoride bond in molecules such as C$_6$F$_6$ tend to be chemically inert and resistant to processes like oxidative degradation [1]. Generally, fluorocarbons display poor binding affinities, especially for saturated substrates given the lack of π-frameworks that may be susceptible to bind to a metal center [1]. Activating C–F bonds by metal–carbon multiple bonds is conceptually a plausible strategy, but successful execution has proven difficult with the only reported example being promoted by a transient titanium alkylidyne (PNP)Ti≡C^{t}Bu (**A**) (PNP$^-$ = N[2-P(CHMe$_2$)$_2$-4-methylphenyl]$_2$) [2]. Intermediate **A** can cleave the C–F linkage in perfluoro substrates like C$_6$F$_6$ and CF$_3$C$_6$F$_5$ under mild conditions to afford rare examples of disubstituted titanium alkylidene-fluorides, (PNP)Ti=C[^{t}Bu(Ar$_F$)](F) (Ar$_F$=C$_6$F$_5$, **1**; *p*-CF$_3$C$_6$F$_4$, **2**) depicted in Scheme 1 (the drawing of the simplified cartoon represents PNP$^-$).

In both cases, mixtures of *syn* and *anti* alkylidene rotational isomers are observed in solution [2]. ^{31}P NMR spectroscopy allowed the observation of the equilibrium (65:35 ratio of **1** *syn*:*anti*) of these samples when heated at 105 °C for 1 h. Titanium–alkylidene complexes are not known to undergo rotation about the M–L double bond readily and the coexistence of two alkylidene rotamers in equilibrium is an exceedingly rare phenomenon [2,3]. Even though alkylidene isomers for Schrock type alkylidenes are known for the heavier congeners of group 5, 6 and 7 transition metals [4–6], examples of isomers for group 4 transition metals have not been documented until recently [2,3]. Understanding the rotation process is important since knowing how each isomer is favored or disfavored may allow for better controlling the reactivity of the alkylidene catalyst formed in reaction (e.g. alkene metathesis and the polymerization of cyclic olefins). This feature is especially true since it is now well documented that alkylidene isomers have different reactivity and selectivity [4–6]. For instance, Schrock found that the *anti* alkylidene isomer of (RO)$_2$Mo=NAr(CHCMe$_2$Ph) (R = OCMe$_3$, OCMe$_2$(CF$_3$), OCMe(CF$_3$)$_2$, OC(CF$_3$)$_2$(CF$_2$CF$_2$CF$_3$); Ar = 2,6-^{i}Pr$_2$C$_6$H$_3$), is at least two orders of magnitude more reactive for the ring-opening metathesis of bis(trifluoromethyl)norbornadiene than the corresponding *syn* isomer [5]. It has been argued that the barrier to

* Corresponding authors. Fax: +1 812 855 8300.
  E-mail address: mindiola@indiana.edu (D.J. Mindiola).
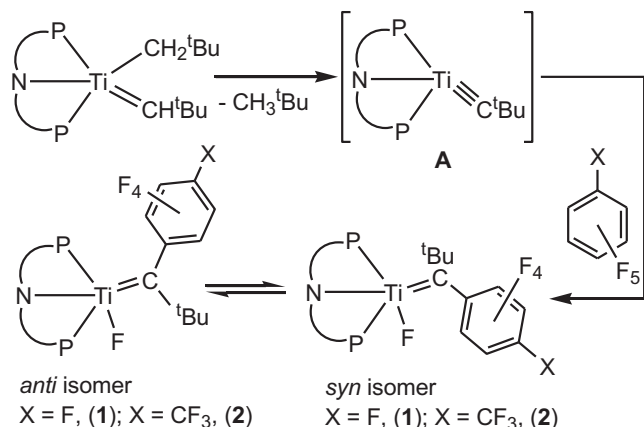
Scheme 1. Synthesis of complexes **1** and **2** (and their respective isomers) from C–F bond activation of C_6F_6 and C_7F_8 via transient $(PNP)Ti \equiv C^tBu$ (**A**). The PNP^- pincer ligand has been simplified to a caricature.

rotation of these alkylidene isomers is sensitive to the availability of a π-type d-orbital orthogonal to the M═C bond as well as an interaction of an α-CH agostic bond with the metal center [4]. To prohibit the interconversion of *syn* and *anti* isomers in solution the groups of Fürstner [7,8] and Grubbs [9,10] prepared tethered ruthenium carbene complexes with carbene ligands connected to an N-heterocyclic carbene. Odom reported the only examples of early-transition metal alkylidene complexes tethered to the adjacent imido ligand (Schrock-type catalysts) [11].

We have shown previously that transient titanium alkylidyne complexes supported by the tridentate PNP ligand $(PNP^- = N[2-P(^iPr)_2-4-methylphenyl]_2)$ can activate C–H bonds present in aromatic and aliphatic substrates [3,12–14]. In addition to promoting intermolecular C–H bonds activation, we have also utilized the highly reactive alkylidyne moiety to activate other strong bonds like the C–F bond of perfluoroaromatics, the C–O bonds in ethers and the aromatic C–N bond in pyridine [2,15–17]. In the case of perfluoroaromatics, we can prepare the disubstituted alkylidene ligands carrying an aliphatic group such as ^tBu, as well as a perfluoroaromatic group on titanium (Scheme 1). These unusual alkylidene complexes exhibit very long Ti═C distances and exist as alkylidene rotational isomers in solution [2]. The goal of this study is to understand how a titanium alkylidyne, **A**, activates the C–F bond of perfluoroarenes (hexafluorobenzene and octa-fluorotoluene) but also to elucidate the mechanism behind formation of the two titanium alkylidene rotational isomers.

2. Experimental details

2.1. General considerations

Unless otherwise stated, all operations were performed in an M. Braun Lab Master double-dry box under an atmosphere of purified nitrogen or using high vacuum standard Schlenk techniques under an argon atmosphere. Non-protic solvents such as *n*-hexane, *n*-pentane, toluene, benzene, and Et_2O were dried according to literature procedures [18]. Deutero solvents were purchased from Cambridge Isotope Laboratory (CIL), degassed and vacuum transferred to 4 Å molecular sieves. Celite, alumina, and 4 Å molecular sieves were activated under vacuum overnight at 200 °C. Compound $(PNP)Ti═CH^tBu(CH_2^tBu)$, was prepared according to the literature [13]. The non-optimized syntheses of complexes **1** and **2** have been previously communicated [2]. All other solvents used as reagents were dried by passage through an activated alumina column and if necessary, vacuum transferred from a CaH_2 mixture

(which was stirred for 2 days prior to transfer). All other chemicals were used as received. ^1H, ^{13}C, ^{19}F, and ^{31}P NMR spectra were recorded on Varian 400 or 300 MHz NMR spectrometers. ^1H and ^{13}C NMR are reported with reference to residual solvent resonances (7.16 and 128.0 ppm for C_6H_6 in C_6D_6). ^{19}F NMR chemical shifts are reported with respect to external $HOCOCF_3$ (−78.5 ppm). ^{31}P NMR chemical shifts are reported with respect to external H_3PO_4 (aqueous solution, 0.0 ppm).

2.2. Separation of $(PNP)Ti═[C^tBu(C_6F_5)](F)$ (1-syn) from the mixture

In a vial was dissolved $(PNP)Ti═CH^tBu(CH_2^tBu)$ [118 mg, 0.191 mmol] in hexafluorobenzene (~2 mL, excess, passed through a short column of alumina) at room temperature. The solution was allowed to stand for 2 days at 50 °C where the solution changed from green to dark-red. The solution was dried under vacuum and the residue was extracted with pentane and filtered. The filtrate was reduced in volume under reduced pressure, and then cooled to −35 °C. Red and orange crystals of $(PNP)Ti═[C^tBu(C_6F_5)](F)$ (**1**) [108 mg, 0.148 mmol, 78% yield] were collected and the crude ^{31}P NMR spectrum showed a mixture of alkylidene isomers to be in approximately a 65:35 ratio. Fractional crystallization of the solids allowed for isolation of the **1**-*syn* isomer. For (**1**-*syn*, 85% pure with 15% of the *anti* isomer): ^1H NMR (23 °C, 399.8 MHz, C_6D_6): δ 7.18 (br d, 1H, $J_{H-H} = 6.04$ Hz, C_6H_3), 6.86–6.88 (m, 1H, C_6H_3), 6.70–6.77 (m, 3H, C_6H_3), 6.62 (m, 1H, C_6H_3), 2.64–2.76 (m, 1H, CHMe$_2$), 2.41–2.52 (m, 1H, CHMe$_2$), 2.28 (s, 3H, C_6H_3–CH_3), 2.22 (m, 1H, CHMe$_2$), 2.05 (s, 3H, C_6H_3–CH_3), 1.73–1.84 (m, 1H, CHMe$_2$), 1.48–1.59 (m, 6H, CHMe$_2$), 1.47 (s, 9H, Ti═CCMe$_3$), 1.34 (dd, 3H, $J_{P-H} = 14.70$ Hz, $J_{H-H} = 7.14$ Hz, CHMe$_2$), 1.26 (dd, 3H, $J_{P-H} = 13.19$ Hz, $J_{H-H} = 6.87$ Hz, CHMe$_2$), 1.14 (dd, 3H, $J_{P-H} = 15.25$ Hz, $J_{H-H} = 7.15$ Hz, CHMe$_2$), 1.00 (dd, 3H, $J_{P-H} = 14.56$ Hz, $J_{H-H} = 6.87$ Hz, CHMe$_2$), 0.86 (dd, 3H, $J_{P-H} = 14.97$ Hz, $J_{H-H} = 7.15$ Hz, CHMe$_2$), 0.72 (dd, 3H, $J_{P-H} = 12.91$ Hz, $J_{H-H} = 7.14$ Hz, CHMe$_2$). ^{13}C NMR (23 °C, 100.6 MHz, C_6D_6): δ 317.0 (Ti═C$^tBuC_6F_5$), 160.2 (d, C_6H_3), 155.9 (dd, C_6H_3), 133.1 (C_6H_3), 132.9 (C_6H_3), 132.8 (C_6H_3), 132.0 (C_6H_3), 131.8 (d, C_6H_3), 126.7 (d, C_6H_3), 124.4 (d, C_6H_3), 121.5 (d, C_6H_3), 119.7 (d, C_6H_3), 114.1 (d, C_6H_3), 48.2 (Ti═CCMe$_3C_6F_5$), 31.1 (Ti═CCMe$_3C_6F_5$), 25.3 (d, CHMe$_2$), 23.4 (d, CHMe$_2$), 22.1 (d, CHMe$_2$), 21.0 (CHMe$_2$), 20.4 (CHMe$_2$), 20.3 (d, CHMe$_2$), 19.5 (C_6H_3–CH$_3$), 19.2 (C_6H_3–CH$_3$), 18.8 (d, CHMe$_2$), 18.0 (d, CHMe$_2$), 17.9 (CHMe$_2$), 17.7 (CHMe$_2$), 17.4 (d, CHMe$_2$), 16.1 (d, CHMe$_2$). The aryl carbon resonances of the C_6F_5 were broad and poorly defined and thus were not included. ^{31}P NMR (23 °C, 121.5 MHz, C_6D_6): δ 33.1 (dd, $J_{P-P} = 40$ Hz, $J_{P-F} = 20$ Hz), 18.7 (dd, $J_{P-P} = 40$ Hz, $J_{P-F} = 20$ Hz). ^{19}F NMR (23 °C, 282.3 MHz, C_6D_6): δ 195.3 (t, $J_{P-F} = 29$ Hz, Ti–F), −133.1 (br s, Ti═C$^tBuC_6F_5$), −163.3 (t, Ti═C$^tBuC_6F_5$), −166.6 (t, 2F, Ti═C$^tBuC_6F_5$).

For the mixture of **1**: ^1H NMR (23 °C, 399.8 MHz, C_6D_6): δ 7.15 (d), 7.00 (d), 6.97 (d), 6.87 (d), 6.84 (d), 6.76 (d), 6.69, 6.70, 6.65, 6.64, 6.63, 6.61, 6.60, 6.59, 6.58, 2.84 (septet), 2.71 (septet), 2.45 (septet), 2.28, 2.25, 2.23, 2.05, 2.01, 1.77 (septet), 1.58, 1.56, 1.54, 1.53, 1.52, 1.44, 1.43, 1.41, 1.40, 1.37, 1.355, 1.33, 1.31, 1.30, 1.28, 1.26, 1.24, 1.07, 1.06, 1.04, 0.98, 0.96, 0.89, 0.87, 0.85, 0.82, 0.79, 0.74, 0.72, 0.70, 0.69. ^{13}C NMR (23 °C, 100.6 MHz, C_6D_6): δ 323.5, 317.0, 160.3 (d), 159.0 (d), 155.9 (dd), 153.7 (dd), 133.1, 132.9, 132.8, 132.7, 132.0, 131.8 (d), 130.6 (d), 126.8 (d), 126.7 (d), 125.2 (d), 124.4, 123.2 (br t), 122.4 (d), 121.7 (d), 121.5 (d), 119.6 (d), 114.1 (d), 114.0 (d), 48.2, 45.6, 32.9, 31.1, 26.0 (d), 25.3 (d), 23.9 (d), 23.5, 23.4, 23.4, 23.3, 23.2, 23.0, 22.9, 22.7, 22.1 (d), 21.0, 20.9, 20.4, 20.3, 19.5, 19.5, 19.4, 19.3, 19.2, 19.0, 18.7, 18.0, 17.7, 17.4 (d), 16.1 (d). ^{31}P NMR (23 °C, 121.5 MHz, C_6D_6): δ 33.1 (dd, $J_{P-P} = 39$ Hz, $J_{P-F} = 21$ Hz), 32.0 (ddd, $J_{P-P} = 42$ Hz, $J_{P-F} = 23$ Hz, $J_{P-F'} = 6$ Hz), 19.6 (dd, $J_{P-P} = 39$ Hz, $J_{P-F} = 21$ Hz), 18.7 (ddd, $J_{P-P} = 42$ Hz, $J_{P-F} = 23$ Hz, $J_{P-F'} = 6$ Hz). ^{19}F NMR (23 °C, 282.3 MHz,

C_6D_6): δ −131.4 (d), −133.1 (br s), −134.2 (d), −161.9 (t), −163.4 (t), −165.5 to −165.3 (m), −166.7 (br t), −166.9, −166.8 (m).

2.3. Preparation of (PNP)Ti=[$C^tBu(C_7F_7)$](F) (2-syn/2-anti)

In a vial was dissolved (PNP)Ti=CH^{t}Bu(CH$_2^t$Bu) [101 mg, 0.164 mmol] in octafluorotoluene ($\sim$2 mL, excess, passed through a short column of alumina) at room temperature. The solution was allowed to stand for 2 days at 50 °C where the solution changed from green to dark-red. The solution was dried under vacuum and the residue was extracted with pentane and filtered. The filtrate was reduced in volume under reduced pressure, and then cooled to −35 °C. Orange crystals of the *syn* isomer (PNP)Ti=[$C^tBu(C_7F_7)$](F) **2**-*syn* [78 mg, 0.100 mmol, 61% yield] were collected but these are always marred with significant amount of the *anti* isomer (dark orange).

For **2**-*syn*: Crystals were manually picked from the crude mixture and analyzed by multinuclear NMR. ^{1}H NMR (23 °C, 399.8 MHz, C_6D_6): δ 7.19 (br d, 1H, J_{H-H} = 5.77 Hz, C_6H_3), 6.85−6.88 (br d, 2H, J_{H-H} = 7.42 Hz, C_6H_3), 6.66−6.72 (m, 2H, C_6H_3), (m, 1H, C_6H_3), 2.62−2.74 (m, 1H, CHMe$_2$), 2.37−2.49 (m, 1H, CHMe$_2$), 2.31 (C_6H_3−CH_3), 2.15−2.29 (m, 1H, CHMe$_2$), 2.05 (C_6H_3−CH_3), 1.71−1.83 (m, 1H, CHMe$_2$), 1.44−1.55 (m, 6H, CHMe_2), 1.43 (s, 9H, Ti=CHCC$Me_3C_7F_7$), 1.32 (dd, 3H, J_{P-H} = 14.83 Hz, J_{H-H} = 7.14 Hz, CHMe_2), 1.23 (dd, 3H, J_{P-H} = 13.46 Hz, J_{H-H} = 6.87 Hz, CHMe_2), 1.12 (dd, 3H, J_{P-H} = 10.17 Hz, J_{H-H} = 6.87 Hz, CHMe_2), 0.99 (dd, 3H, J_{P-H} = 14.70 Hz, J_{H-H} = 6.86 Hz, CHMe_2), 0.86 (dd, 3H, J_{P-H} = 15.94 Hz, J_{H-H} = 7.15 Hz, CHMe_2), 0.70 (dd, 3H, J_{P-H} = 12.91 Hz, J_{H-H} = 7.14 Hz, CHMe_2). ^{31}P NMR (23 °C, 121.5 MHz, C_6D_6): δ 33.3 (dd, J_{P-P} = 53 Hz, J_{P-F} = 27 Hz), 18.9 (dd, J_{P-P} = 53 Hz, J_{P-F} = 27 Hz). ^{19}F NMR (23 °C, 282.3 MHz, C_6D_6): δ −55.9 (m, 3F), −131.8 (s, 2F), −145.1 (m, 2F).

Assignment of the mixture of the two isomers was not possible, therefore only resonances and multiplicity when known are given. ^{1}H NMR (23 °C, 399.8 MHz, C_6D_6): δ 7.18 (br d), 7.14 (d), 7.01, 6.99, 6.95−6.96 (m), 6.79−6.87 (m), 6.57−6.71 (m), 2.82 (septet), 2.67 (septet), 2.42 (septet), 2.31, 2.27, 2.22 (septet), 2.19, 2.06, 2.03, 2.00, 1.77 (septet), 1.46−1.55 (m), 1.42, 1.21−1.40 (m), 1.13 (dd), 1.03, 1.01, 0.98 (dd), 0.78−0.89 (m), 0.70 (dd). ^{13}C NMR (23 °C, 100.6 MHz, C_6D_6): δ 320.6, 315.7, 160.2 (d), 158.8 (d), 155.8 (d), 153.2 (dd), 133.7, 133.2, 133.1, 133.1, 132.9, 132.1, 132.0, 131.8 (d), 130.7, 127.2 (d), 126.9 (d), 124.8, 124.5, 124.4, 124.3, 122.7 (d), 122.1, 122.0, 121.8, 121.6, 121.3, 119.7 (d), 114.2, 114.1, 114.0, 113.9, 48.2, 45.6, 33.0, 31.2, 31.1, 26.0 (d), 25.3 (d), 25.1 (d), 24.5 (d), 23.9 (d), 23.5, 23.4, 22.9, 22.8, 22.7, 22.3, 22.0, 21.9, 21.0, 20.8, 20.6, 20.5, 20.4, 20.3, 20.2, 19.4, 19.3, 19.2, 19.0, 18.9, 18.7, 18.0, 17.9, 17.8, 17.7, 17.5, 17.3, 17.2, 17.1, 16.1 (d). ^{31}P NMR (23 °C, 121.5 MHz, C_6D_6): δ 33.3 (dd, J_{P-P} = 53 Hz, J_{P-F} = 27 Hz), 31.5−32.9 (m), 19.4−20.2 (m), 18.9 (dd, J_{P-P} = 53 Hz, J_{P-F} = 27 Hz). ^{19}F NMR (23 °C, 282.3 MHz, C_6D_6): δ −55.7 (m), −55.9 (m), −108.3, −108.9 (br s), −117.5 (d), −117.9 (m), −118.9 (d), −140.5 (m), −141.3 to −141.0 (m), −142.7 (m), −144.4 (m), −145.5 to −145.2 (m), −147.9 (m), −160.3 (m), −164.6 (m), −165.4 (m), −166.2 (m).

2.4. Computational details

All calculations were carried out using Density Functional Theory as implemented in the Jaguar 7.0 suite [19] of ab initio quantum chemistry programs. Geometry optimizations were performed with the B3LYP [20−22] functional and the 6-31G** basis set with no symmetry restrictions. This protocol has been shown to be a reasonable compromise between model accuracy and computational cost for transition metal-containing systems [23]. All transition metals were represented using the Los Alamos basis set (LACVP) [24,25]. Energies of the optimized structures were reevaluated by additional single-point calculations on each optimized

geometry using Dunning's correlation-consistent triple-ζ basis set [26], cc-pVTZ(-f). For all transition metals we used a modified version of LACVP, designated LACV3P, in which the exponents were decontracted to match the effective core potential with the triple-ζ quality basis. Vibrational frequency calculations based on analytical second derivatives at the B3LYP/6-31G** (LACVP) level of theory were carried out to derive the zero-point-energy (ZPE) and entropy corrections at room temperature (unless otherwise noted) utilizing unscaled frequencies. Full models were used in our calculations and for simplicity, the rotation study was conducted using the isomers of **1** only, as **2** differs only by having a CF_3 para substituent on the perfluorinated phenyl ring.

3. Results and discussion

Activation of C−F bonds by metal−carbon multiple bonds is exceedingly rare with the only reported example being the transient titanium alkylidyne (PNP)Ti≡C^{t}Bu (**A**) (PNP$^-$ = N[2-P(CHMe$_2$)$_2$-4-methylphenyl]$_2$) [2]. Species **A** can cleave the C−F linkage in perfluoro substrates like C_6F_6 and C_7F_7 under mild conditions to afford disubstituted alkylidene-fluorides, (PNP)Ti=C[^{t}Bu(Ar$_F$)](F) (Ar$_F$ = C_6F_5, **1**; C_7F_7, **2**) depicted in Scheme 1 (the lines represents PNP$^-$) [2]. In both cases, mixtures of *syn* and *anti* alkylidene isomers are observed in solution. In the case of complex **1**, fractional crystallization allowed for crystallographic characterization of the *syn* rotamer, (PNP)Ti=C[^{t}Bu(C_6F_5)](F), and in the case of complex **2**, both the *syn* and *anti* isomers of (PNP)Ti=C[^{t}Bu(C_7F_7)](F) could be physically separated based on their distinctively different colors. At various temperatures it was also confirmed that these rotational isomers slowly interconvert [2]. To our knowledge, the only other example of a 1,2-CF bond activation by a metal−ligand multiple bond was reported by Bergman and co-workers using the racemic ansa-metallocene imido rac-(ethylenebis(tetrahydro)indenyl)Zr=N^{t}Bu (generated in solution) and NC$_5$F$_5$, to yield the amide fluoride (ethylenebis(tetrahydro)indenyl)Zr(N^{t}Bu[NC$_5$F$_4$])F (Eq. (1)) [27]. In such a reaction, the C−F breaking event was proposed to be driven by a combination of the inherent reactivity of the pyridine C−F motif as well as formation of a very strong Zr−F bond. Naturally, one would predict Bergman's activation of NC$_5$F$_5$ to obey an analogous pathway for the C−F bond breaking event observed between transient **A** and the perfluoroarene given that a metal−ligand multiple bond is responsible. However, the nature of the substrates, perfluoropyridine versus perfluorobenzene, should render these two reactions fundamentally different. For example, *N*-coordination of the perfluoropyridine substrate to the metal center most likely plays an important role along the bond-breaking event, which cannot be present in the case of the perfluoroarene.

To assess whether or not binding of the substrate could alter the pathway along the C−F activation reaction we explored two types of mechanistic scenarios for the formation of the alkylidene fluoride, **1**-*syn*, computationally using DFT and focusing on the substrate C_6F_6. As noted above, Bergman and co-workers reported the C−F activation of NC$_5$F$_5$ by racemic (ethylenebis(tetrahydro)indenyl)Zr=N^{t}Bu, but the mechanism leading to C−F bond cleavage in the substrate was not discussed [27]. If binding of the pyridine followed by cycloaddition of the *N*-heterocycle were the steps preceding the C−F bond activation reaction, then a β-fluoride elimination process should be dominating. On the other hand, formation of the alkylidene species **1** and **2** shown in Scheme 1 may proceed by a more direct 1,2-CF addition across the Ti≡C or may involve initial coordination of the fluorine followed by migration of the aryl carbon to the

(Eq. 1)
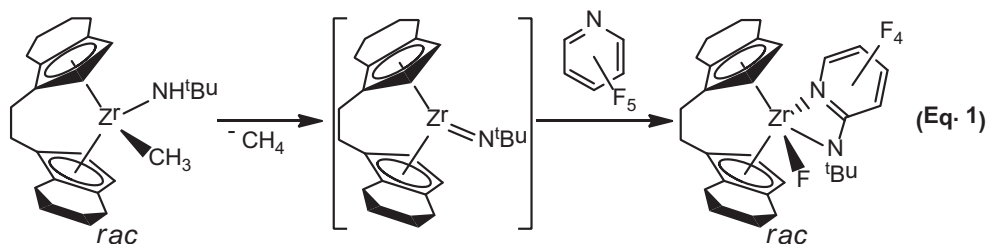
alkylidyne carbon. Experimentally discerning which pathway is involved is virtually impossible due to the difficulty in isotopically labeling both the C or F sites among many other problems. Previous studies established that formation of $(PNP)Ti\equiv C^tBu$ is often rate-determining based on our KIE values obtained for the rates of $(PNP)Ti=CH^tBu(CH_2^tBu)/(PNP)Ti=CD^tBu(CD_2^tBu)$ along the C−H activation of benzene, hydrocarbons, and hydrofluoroarenes (KIE = 3.7, 27 °C) [3,12−14] as well as the activation and ring-opening metathesis of pyridine (KIE = 3.8(3), 25 °C) [15]. Therefore, experimentally investigating steps after the elimination of CH_3^tBu could yield little mechanistic information.

The solid line depicted in Fig. 1 represents the most energetically accessible pathway for 1,2-CF addition of C_6F_6 across the $Ti\equiv C^tBu$ ligand of **A**. Transient **A** is 4.6 kcal/mol higher in energy than $(PNP)Ti=CH^tBu(CH_2^tBu)$ and coordination of C_6F_6 to $(PNP)Ti\equiv C^tBu$ can be accomplished at an energy cost of 14.1 kcal/mol to form the putative adduct $(PNP)Ti\equiv C^tBu(\sigma\text{-}C_6F_6)$ (**A1**) (overcoming a simulated barrier, labeled with a star *, which we were not able to compute with standard methods and is therefore estimated), which then undergoes a virtually barrierless 1,2-CF addition step with a penalty of ∼3.7 kcal/mol to produce the *syn* isomer of **1**. Although the overall C−F activation barrier is 22.4 kcal/mol, this value is considerably lower than the α-abstraction to form **A** (27.8 kcal/mol). It is not obvious whether the binding event or the activation of the C−F bond would be more difficult. However, given that **A-TS** is much higher in energy than **A1** by 9.1 kcal/mol we are confident to state that α-abstraction to form **A** is overall rate-

determining in this type of reaction, as we have observed in many other reactions (the rates of these reactions are also similar with a $t_{1/2}$ in ∼3.1 h at room temperature).

The computed pathway depicted by a dashed line also presents a coordination event (**A1′**), followed by a stepwise process invoking first a [2 + 2]-cycloaddition of C_6F_6 to form the metallacyclobutene intermediate $(PNP)Ti(C^tBu[C_6F_6])$ (**A2**), which then β-fluoride eliminates to yield **1**-*syn*. Although an intermediate invoking the facial binding of the π-system in C_6F_6 may exist, we were unable to locate this intermediate labeled as **A1′** with our current theoretical methods. We marked this putative reactant complex with a "?" in Fig. 1 and placed it at a reasonable energy on the reaction coordinate for illustration. The formation of **A** to **A2** should therefore be best viewed as a concerted [2 + 2]-cycloaddition step with an overall energy cost of 26.2 kcal/mol. Interestingly, **A2** is almost isoenergetic with **A**, but the β-fluoride elimination step is extremely facile with a barrier of only 4.3 kcal/mol. In this pathway we cannot estimate the energy for **A1′**, but we propose the cycloaddition barrier to be the slowest step along the C−F bond-breaking event since the energy to traverse from **A** to **A2** is at least 26.2 kcal/mol. Although the $\Delta\Delta G^{\ddagger}$ between 1,2-CF bond addition and [2 + 2]-cycloaddition/β-fluoride elimination is relatively small (3.8 kcal/mol), we propose that 1,2 addition is the more facile pathway since the energy difference between **A1′-TS**, which we were able to locate, and **A1** is substantial at 7.5 kcal/mol.

As illustrated in Fig. 1, the C_6F_6 substrate binds to the Ti(IV) center in an electrostatic fashion using F as the contact atom.
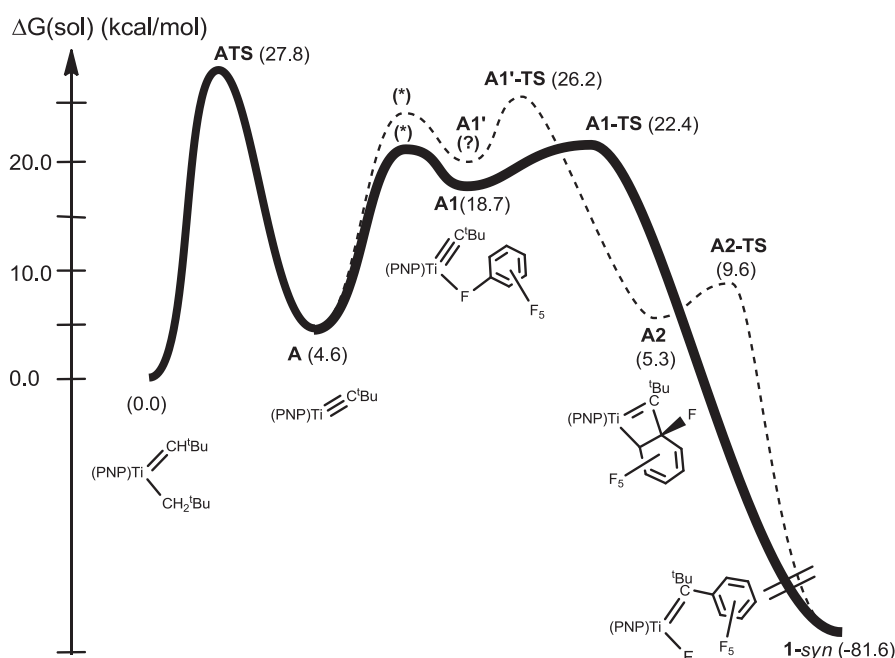
Fig. 1. Two distinct C−F bond activation pathways of the substrate C_6F_6 via transient **A**.

Table 1
ESP charge variations for the 1,2-CF activation pathway involving the substrate C_6F_6.

	Ti	F1	C1	C2	C_6F_6
Adduct (**A1**)	0.91	0.02	−0.12	−1.25	0.10
TS (**A1-TS**)	1.16	−0.14	−0.03	−1.03	−0.17
Δq	+0.25	−0.12	+0.09	+0.22	−0.27

Table 1 summarizes the substantial distortion of the electrostatic potential (ESP) that the adduct formation affords in terms of the ESP-fit charge variations. Fig. 2 depicts the computed structures of the transition state structure **A1-TS**. Structurally, **A1-TS** can be considered early as the Ti≡C2 and C1−F bonds are only slightly elongated from that of **A** and free C_6F_6, respectively. Fig. 2 also illustrates the proposed structure for the [2 + 2]-cycloaddition
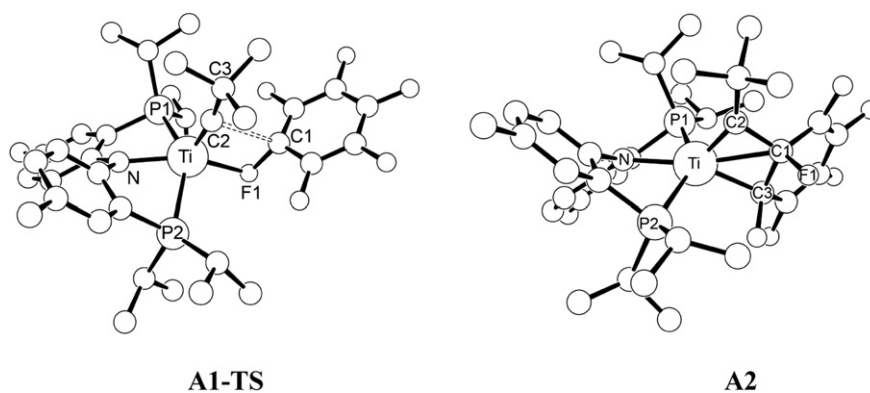
Fig. 2. Computed transition state in 1,2-C−F addition pathway leading to **1**-*syn* (**A1-TS**) and computed structure of the intermediate **A2** involved in the cycloaddition pathway leading to C−F activation. Distances are reported in Å. For **A1-TS**: Ti−F1, 2.14; Ti−C2, 1.76; Ti−P1, 2.64; Ti−P2, 2.63; Ti−N, 2.06; F1−C1, 1.46; C1−C2, 2.56. For **A2**: Ti−F1, 2.43; Ti−C2, 1.75; Ti−P1, 2.62; Ti−P2, 2.59; Ti−N, 2.09.
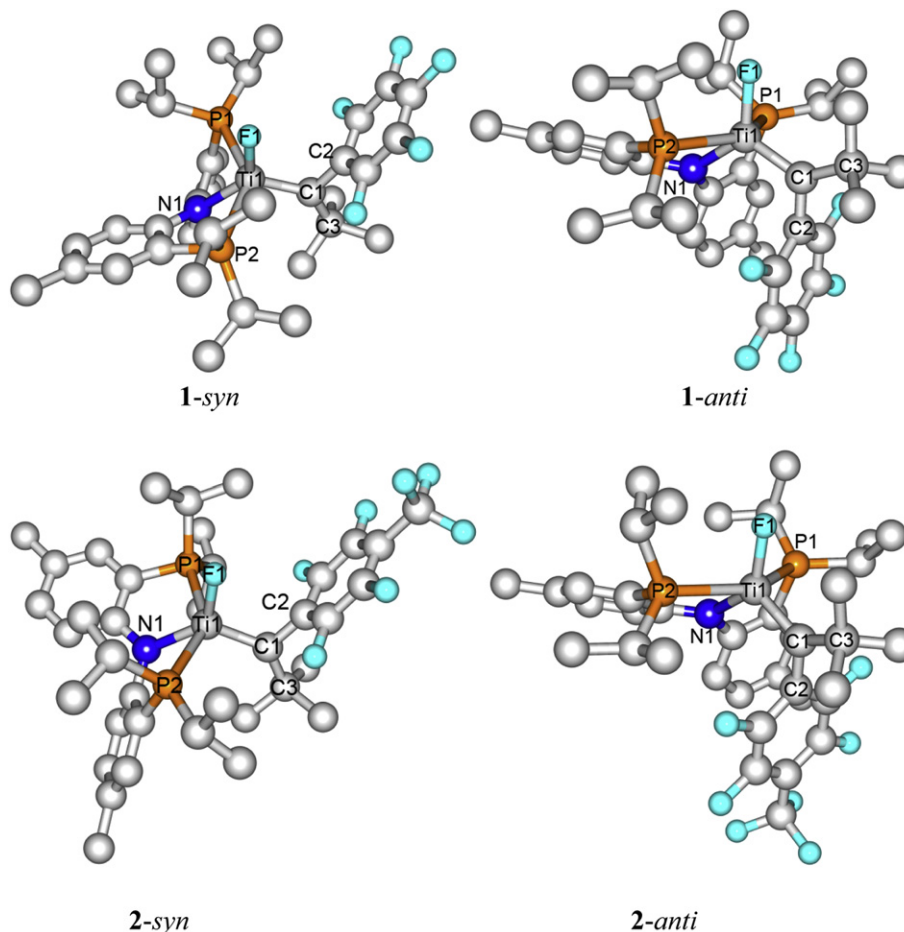
Fig. 3. Molecular models of the *syn* and *anti* isomers of (PNP)Ti=[C^{t}Bu(C$_6$F$_5$)](F) (**1**) and (PNP)Ti=[C^{t}Bu(C$_7$F$_7$)](F) (**2**). Hydrogen atoms have been omitted for clarity.

Table 2
Comparison of selected bond distances (Å) and angles (°) in DFT-optimized and crystal structures of **2**-*syn* and **2**-*anti*.

Bond/angle	1-*syn*		1-*anti*	2-*syn*		2-*anti*	
	DFT	X-ray	DFT	DFT	X-ray	DFT	X-ray
Ti1−P1	2.620	2.6049 (7)	2.630	2.623	2.5986 (6)	2.624	2.5610 (5)
Ti1−P2	2.658	2.6050 (7)	2.662	2.658	2.6181 (5)	2.657	2.6251 (5)
Ti1−N1	2.065	2.0566 (17)	2.055	2.061	2.0517 (14)	2.053	2.0491 (14)
Ti1−F1	1.802	1.8211 (12)	1.800	1.800	1.8287 (10)	1.800	1.8166 (10)
Ti1−C1	1.919	1.946 (2)	1.920	1.922	1.9487 (18)	1.925	1.9510 (17)
C1−C2	1.500	1.503 (3)	1.497	1.495	1.496 (2)	1.492	1.493 (2)
C1−C21	1.547	1.541 (3)	1.551	1.549	1.544(2)	1.554	1.536 (2)
P1−Ti1−P2	145.45	144.80 (2)	143.10	145.19	145.294 (19)	142.76	142.304 (18)
N1−Ti1−F1	128.60	133.27 (6)	130.37	129.20	132.88 (5)	132.46	137.48 (5)
F1−Ti1−C1	109.34	106.89 (7)	113.11	108.42	105.64 (6)	112.54	111.89 (6)
C2−C1−C3	115.71	114.30 (17)	115.32	115.61	115.97 (14)	115.32	114.39 (14)
N1−Ti1−C1	121.92	119.73 (8)	116.62	122.21	121.28 (7)	114.99	110.63 (6)
F1−Ti1−C1−C2	−5.15	5.43 (16)	−175.67	−8.08	−6.03 (13)	−173.75	−174.89 (11)

product for C_6F_6, **A2**, where the carbon C1 has been hybridized to sp^3, while the bond order calculations suggest the C1−F bond of this intermediate to be much weaker relative to the value computed for the free substrate, C_6F_6. As noted previously, we were unable to locate a minimum for the structure of a π-bound adduct of **A** with C_6F_6 (**A1′**) which ultimately undergoes a [2 + 2]-cyclo-addition to form **A2** followed by β-fluoride elimination to generate **1**-*syn*.

To better understand the electronic structure of **1** and investigate the mechanism of rotation of the alkylidene ligands from *syn* to *anti*, it is instructive to first compare the DFT-optimized structures of alkylidene complexes **1** and **2** in their isomeric forms *syn* and *anti*, where *syn* is the isomer where the C_6F_5 fragment is oriented to the same side as the fluoride ligand. The computed structures are shown in Fig. 3. The computed isomeric forms of **2** could be compared to the corresponding crystallographic structures of **2**-*syn* and **2**-*anti* which have been published elsewhere [2]. Both systems were found to be in good agreement with the metrical parameters obtained from their crystal structures (Table 2). As anticipated, bond lengths and angles for both isomers

of **2** and **1**-*syn* are comparable which also places them really close in energy at $\Delta E(SCF) = 2.0$ kcal/mol. For structural comparison we focused our attention on complex **2** since single crystals suitable for X-ray diffraction studies could be grown for both isomeric forms (unfortunately only the *syn* isomer of **1** could be structurally confirmed) [2]. The computed structures of the *syn* isomers of **1** and **2** are quite similar. In complex **2**-*syn*, the molecular structure reveals the Ti=C distance (Ti1−C1) of 1.9487(18) Å and elongates slightly to 1.9510(17) Å for **2**-*anti* (Table 1), while in **2**-*syn*, the Ti=C distance in **1**-*syn* is 1.946(2) Å. For **1**, the alkylidene isomers have a dihedral angle between F1−Ti1−C1−C2 of 0° in **1**-*syn* and changes to 178.87° in **1**-*anti*. The bond between Ti1−F1 decreases negligibly from the *syn* to the *anti* isomer (1.806 Å to 1.799 Å, respectively).

An experimental study of the isomerization process was performed using complex **1**, since the *syn* isomer could be more conveniently separated from the reaction mixture, therefore allowing us to enrich a solution with approximately 85/15 mixture of *syn* and *anti* isomers, respectively [2]. After refluxing this sample for 1 h in benzene at 105 °C the ratio converted to 65/35 (*syn*/*anti*).
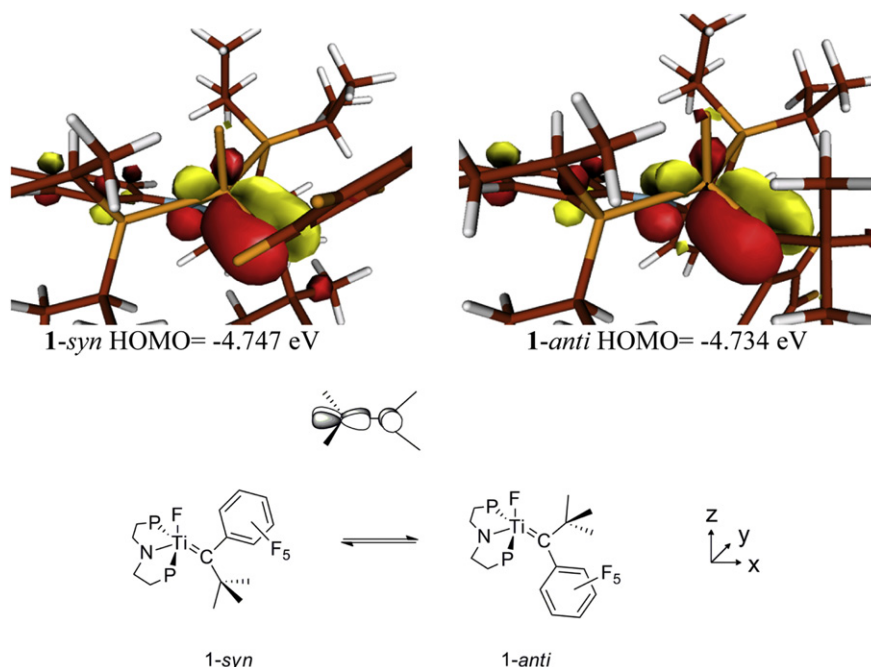
Fig. 4. HOMO of **1**-*syn* and **1**-*anti* with isodensity value of 0.05 au and schematic representation of the participating orbitals.
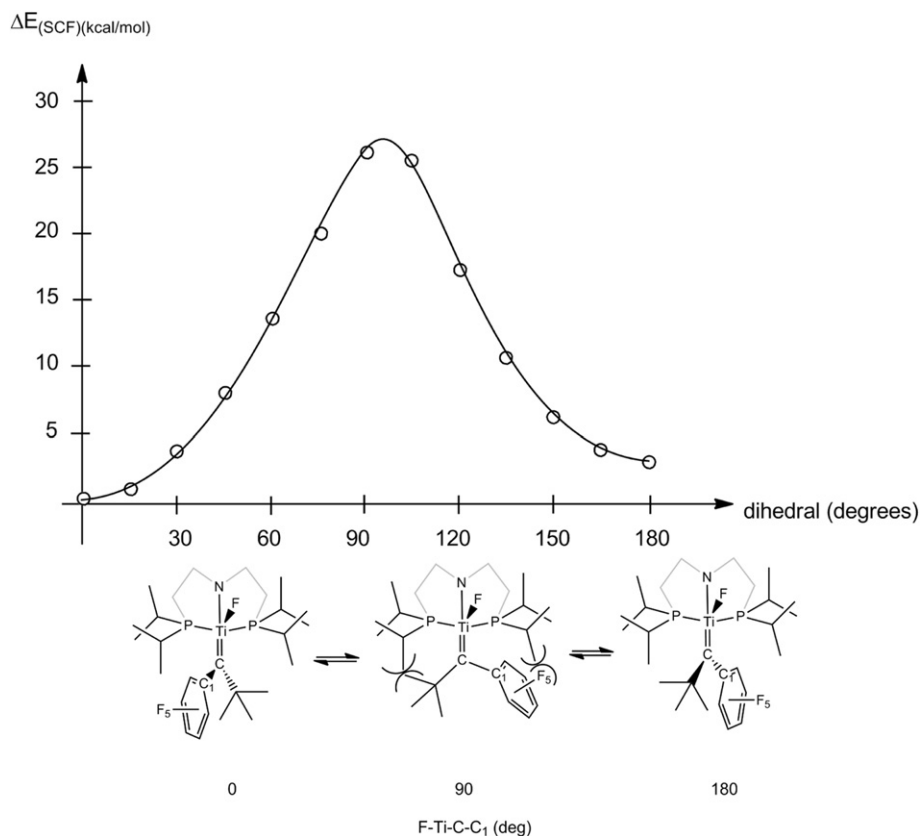
Fig. 5. Plot of the electronic energy versus rotation about the titanium–alkylidene ligand of **1** (top) and schematic representation of the mechanism for rotation of the alkylidene ligand from **1**-*syn* at 0° to **1**-*anti* at 180° (phenylene backbone of the pincer ligand and hydrogen atoms have been eliminated for clarity).

The formation of the two isomers (*syn*/*anti*) is manifested by two distinct alkylidene resonances in the ^{13}C NMR spectrum (323.5 and 317.0 ppm). Likewise, the ^{31}P NMR spectrum confirms two C_1 symmetric species in solution with an average J_{PF} value of 20 Hz. From our theoretical study, the calculated difference in electronic energy between **1**-*syn* and **1**-*anti* isomers is estimated to be 2.5 kcal/mol with **1**-*syn* being slightly favored thermodynamically.

To understand the mechanism of rotation of the alkylidene ligand in **1** and **2**, an orbital analysis of the most important orbitals was conducted. The MO analysis of the frontier orbitals reveals not surprisingly that the HOMO of both **1**-*syn* and **1**-*anti* is involved in the multiple bonding between Ti=C, and can be assigned to the in-phase π interaction between d_{xy} and the corresponding p orbital of the alkylidene carbon (Fig. 4). Only minor changes are observed on common structural metric parameters of both isomers (Table 2). A scan of the potential energy surface associated with the rotational motion to transform **1**-*syn* to **1**-*anti* reveals that the electronic energy of the complex reaches a maximum at 26 kcal/mol when the dihedral angle between F1–Ti1–C1–C2 is 90° (Fig. 5). Whereas the position of the maximum is not surprising its relative energy of

26 kcal/mol is lower than intuitively expected. A video of the rotation from *syn* to *anti* isomerization is available in the supporting information.

Intuitively, the twisting motion that the M–alkylidene moiety must undergo to convert **1**-*syn* to **1**-*anti* is expected to be associated with a higher barrier, because the M–alkylidene double bond must break at the transition state. This process can be envisioned to take place either in a heterolytic or homolytic fashion. The heterolytic Ti=C bond breaking may traverse an electronic structure that formally resembles a Ti^{IV}–C^{1-} fragment where the two electrons from the Ti=C π-orbital are localized on the carbon atom. The alternative charge polarization affording a Ti^{II}–C$^+$ moiety where the two electrons are placed on Ti is less appealing, as it would formally constitute a reductive elimination process that is difficult to envision. In either case, the two π-electrons remain in the same spatial orbital and the overall spin state will be a closed-shell singlet throughout the twisting motion. The homolytic π-bond cleavage, on the other hand, must invoke an open-shell singlet involving an electronic structure that formally contains a Ti^{III}–C•

Table 3
Comparison of selected bond lengths (Å) of DFT-models *syn*, *anti* and 90°-rotated isomers of **1**.

Bond	**1**-*syn*	90°-rotated	**1**-*anti*
Ti1–N1	2.064	2.099	2.049
Ti1–F1	1.802	1.823	1.800
Ti1–P1	2.623	2.663	2.630
Ti1–P2	2.655	2.726	2.662
Ti1–C1	1.918	1.886	1.920

Table 4
Changes in Mayer bond order of the Ti=C bond distance upon change in dihedral angle F1–Ti1–C1–C$_{ArF}$ in complex **1**.

F1–Ti1–C1–C (°)	Mayer bond order	R(Ti1–C1) (Å)
0 (*syn*)	1.50	1.913
30	1.51	1.913
60	1.51	1.919
90	1.51	1.886
120	1.50	1.895
150	1.50	1.909
180 (*anti*)	1.51	1.918
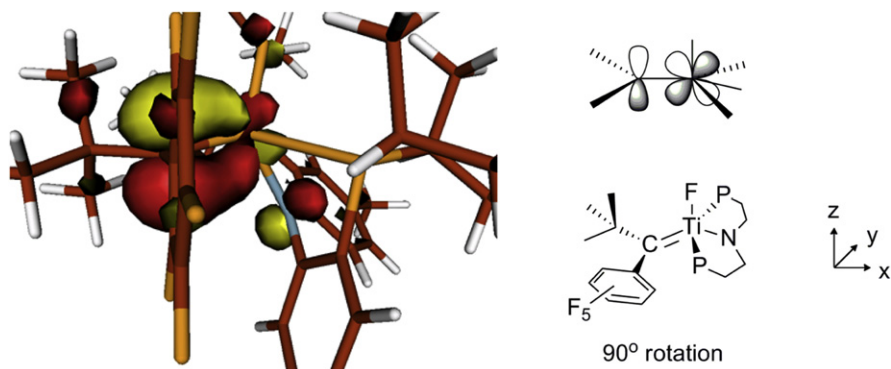
Fig. 6. HOMO (−4.208 eV) of model rotated 90° around the Ti=C bond of **1**-*syn* with isodensity value of 0.05 au.

moiety with the two unpaired electrons adopting opposite spins. Structurally, we expect the Ti···C1 distance to increase at the transition state reflecting on the loss of double bond character. Surprisingly, our calculations indicate that the Ti···C1 decreases upon twisting from 1.918 to 1.886 Å (Table 3). This is a tantalizing result, as we typically correlate M···L distances with bond order and, thus, we may speculate that the double bond character

between the Ti···C1 fragments is maintained throughout the twisting motion, which makes little intuitive sense. One potential reason for such structural anomaly may be that the Ti···C1 distance is not governed by electronics, but by sterics, that is the double bond is formally broken but the metal-ligand distance is enforced by different factors. To test this plausible speculation, we calculated the bond order between titanium and C1 as we varied the twist
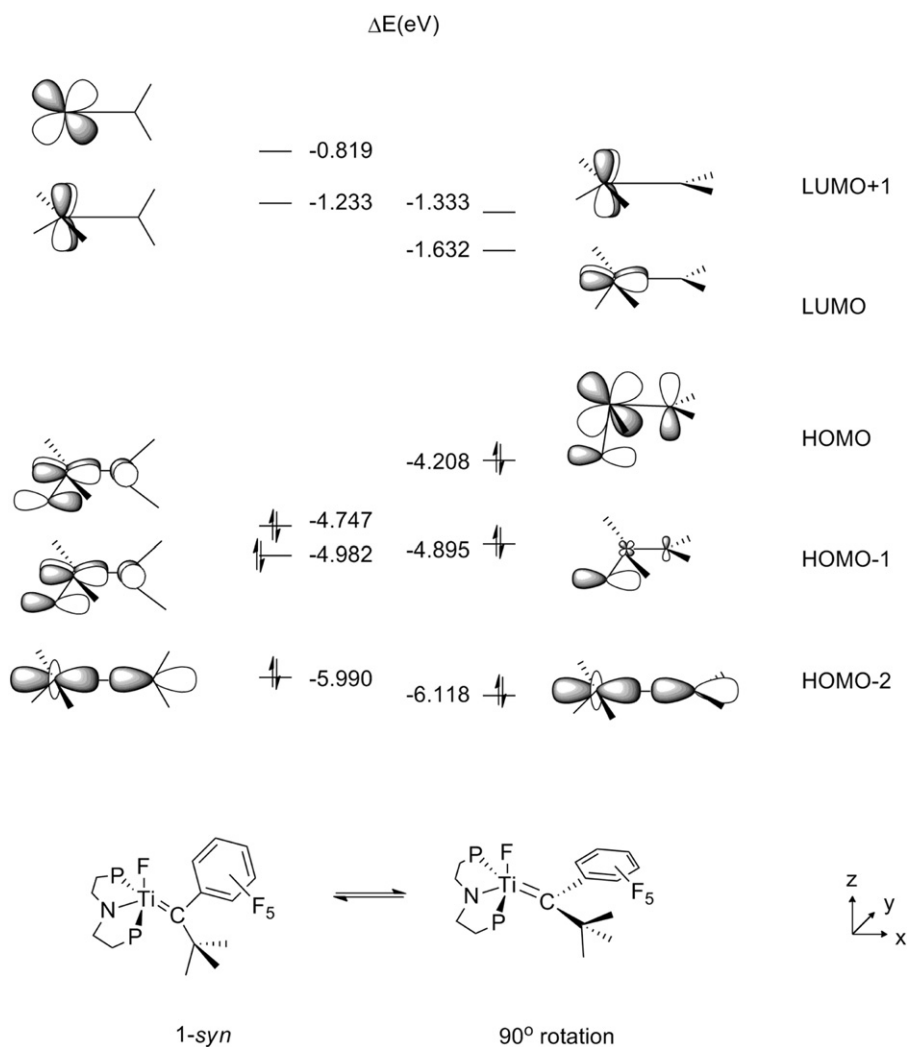
Fig. 7. Molecular orbital redistribution upon 90° rotation of alkylidene ligand in 1-*syn*.

angle, as summarized in Table 4. Throughout the series, the bond order remains identical at 1.5 indicating that the invariance of the Ti···C1 distance arises from the electronic structure of the complex.

A careful inspection of the molecular orbitals reveals finally that the Ti−C π-bonding orbital illustrated in Fig. 4 is indeed maintained at the transition state. Fig. 6 shows the HOMO of the transition state where a twist angle of 90° is adopted. Fig. 7 compares the MO diagrams of **1**-*syn* and the 90-deg rotated transition state. In the transition state structure severe distortion of the PNP ligand backbone characterized by an N1−Ti−C1 angle of 121.92° allows for a different metal-d orbital to serve as the π-acceptor. In **1**-*syn* the π-accepting orbital is d_{xy}, as sketched in Fig. 4, whereas it is the d_{yz} orbital in the transition state geometry that engages and maintains the Ti≡C double bond character as illustrated in Fig. 6. This electronic rearrangement is moderated by the amide nitrogen that is not *trans* to C1, but instead distorts to a *cis* disposition. This electronic flexibility is possible, as all d-orbitals of the Ti(IV)-d^0 center can act as electron acceptors − a flexibility that the organic analogues do not possess. To allow for proper aligning of the appropriate d-π orbital, the observing ligands on Ti must be sufficiently flexible and the PNP backbone fulfills this requirement perfectly. This structural flexibility is the direct result of the softness of the P-atoms. Since Ti(IV) is a hard acid, the Ti−PNP moiety constitutes a soft/hard mismatched construct. As a result, the Ti−P bonds are relatively weak and flexible, resulting in a relatively small energy penalty for structural distortions.

4. Conclusions

In this study we have examined the mechanism to activation of a C−F bond in a perfluoroarene promoted by a transient titanium alkylidyne. Based on the reaction profile we propose the activation of a perfluoroarene to proceed via 1,2-CF bond addition across the Ti≡C bond. We have also investigated the mechanism for the rotation about the Ti≡C bond which gives rise to two isomers, *syn* and *anti*. The *syn* isomer was found to be slightly lower in energy. Surprisingly, we found that the rotation around the Ti≡C bond can be accommodated without breaking the π-bond. Even at the transition state, where the twist angle is 90°, a full π-bond is maintained. This non-intuitive electronic structure is possible, because the Ti(IV)-d^0 can utilize both the d_{xz} and d_{yz} orbitals as the π-accepting orbital. This electronic feature is reminiscent of the situation found in organic acetylene moieties, where rapid rotation is also possible due to the presence of two orthogonal π-orbitals. In this case, the alkylidene fragment that serves as the π-donor only possesses one π-orbital, but the π-accepting fragment has two empty d-π orbitals that can accommodate the Ti≡C twisting. Key to this electronic flexibility is the ease of structural distortion of the PNP backbone that must accommodate a varying ligand environment that in turn affects the metal-d orbital alignment. Although the bulky substituents on both, PNP and alkylidene ligands at first appear to render this rotation an unfavorable process given the severe distortions observed on the chelate's binding to Ti, we conclude that this parameter does not represent a major influence to the energetic penalty.

Acknowledgments

Appendix. Supplementary data

Supplementary data related to this article can be found online at doi:10.1016/j.jorganchem.2011.07.037.

References

[1] (a) B.E. Smart, in: S. Patai, Z. Rappoport (Eds.), The Chemistry of Functional Groups, Supplement D, John Wiley & Sons, New York, 1983 (Chapter 14);
(b) J.L. Kiplinger, T.G. Richmond, C.E. Osterberg, Chem. Rev. 94 (1994) 373;
(c) J. Burdeniuc, R.H. Crabtree, Chem. Ber./Recueil 130 (1997) 145;
(d) W.D. .Jones, Dalton Trans. (2003) 3991;
(e) T.G. Richmond, in: S. Murai (Ed.), Topics in Organometallic Chemistry, vol. 3, Springer, New york, 1999, p. 243.
[2] B.C. Bailey, J.C. Huffman, D.J. Mindiola, J. Am. Chem. Soc. 129 (2007) 5302.
[3] J.A. Flores, V.N. Cavaliere, D. Buck, G. Chen, B. Pinter, M.G. Crestani, M.-H. Baik, D.J. Mindiola, Chem. Science 2 (2011) 1457.
[4] R.R. Schrock, H.H. Fox, M.H. Schofield, Organometallics 13 (1994) 2804.
[5] R.R. Schrock, J.H. Oskam, J. Am. Chem. 114 (1992) 7588.
[6] (a) R.R. Schrock, Polyhedron 14 (1995) 3177 Perfluoroalkylidene isomers of iridium have been reported and recently observed;
(b) J. Yuan, R.P. Hughes, J.A. Golen, A.L. Rheingold, Organometallics 29 (2010) 29 1942;
(c) R.P. Hughes, personal communication.
[7] A. Fürstner, L. Ackermann, B. Gabor, R. Goddard, C.W. Lehmann, R. Mynott, F. Stelzer, O.R. Thiel, Chem. Eur. J. 7 (2001) 3236.
[8] A. Fürstner, H. Krause, L. Ackermann, C.W. Lehmann, Chem. Commun. (2001) 2240.
[9] R.H. Grubbs, C.W. Bielawski, D. Benitez, Science 297 (2002) 2041.
[10] R.H. Grubbs, C.W. Bielawski, D. Benitez, J. Am. Chem. Soc. 125 (2003) 8424.
[11] K.S. Lokare, R.J. Staples, A.L. Odom, Organometallics 27 (2008) 5130.
[12] B.C. Bailey, H. Fan, E.W. Baum, J.C. Huffman, M.-H. Baik, D.J. Mindiola, J. Am. Chem. Soc. 127 (2005) 16016.
[13] B.C. Bailey, H. Fan, J.C. Huffman, M.-H. Baik, D.J. Mindiola, J. Am. Chem. Soc. 129 (2007) 8781.
[14] A.R. Fout, J.L. Scott, D.L. Miller, B.C. Bailey, J.C. Huffman, M. Pink, D.J. Mindiola, Organometallics 28 (2009) 331.
[15] A.R. Fout, B.C. Bailey, D. Buck, H. Fan, J.C. Huffman, M.-H. Baik, D.J. Mindiola, Organometallics 29 (2010) 5409.
[16] B.C. Bailey, H. Fan, J.C. Huffman, M.-H. Baik, D.J. Mindiola, J. Am. Chem. Soc. 128 (2006) 6798.
[17] A.R. Fout, B.C. Bailey, H. Fan, J.C. Huffman, M.-H. Baik, D.J. Mindiola, J. Am. Chem. Soc. 129 (2007) 12640.
[18] A.B. Pangborn, M.A. Giardello, R.H. Grubbs, R.K. Rosen, F.J. Timmers, Organometallics 15 (1996) 1518.
[19] Jaguar, Version 7.0. Schrödinger, L.L.C, New York, NY, 2007.
[20] A.D. Becke, Phys. Rev., A 38 (1988) 3098.
[21] C. Lee, W. Yang, R.G. Parr, Phys. Rev. B 37 (1988) 785.
[22] A.D. Becke, J. Chem. Phys. 98 (1993) 5648.
[23] E.M. Siegbahn, R.A. Blomberg, Chem. Rev. 100 (2000) 421.
[24] P.J. Hay, W.R. Wadt, J. Chem. Phys. 82 (1985) 270.
[25] W.R. Wadt, P.J. Hay, J. Chem. Phys. 82 (1985) 284.
[26] T.H. Dunning, J. Chem. Phys. 90 (1989) 1007.
[27] R.G. Bergman, F.E. Michael, H.M. Hoyt, J. Am. Chem. Soc. 126 (2004) 1018.